Near-Infrared Spectrally Selective Plasmonic Electrochromic Thin Films

ARTICLE *in* ADVANCED OPTICAL MATERIALS · MARCH 2013

Impact Factor: 4.06 · DOI: 10.1002/adom.201200051

6 AUTHORS, INCLUDING:

Guillermo Garcia
Lawrence Berkeley National Laboratory
9 PUBLICATIONS **345** CITATIONS
SEE PROFILE

Raffaella Buonsanti
Lawrence Berkeley National Laboratory
55 PUBLICATIONS **1,574** CITATIONS
SEE PROFILE

Anna Llordés
CIC Energigune
31 PUBLICATIONS **1,117** CITATIONS
SEE PROFILE

ADVANCED OPTICAL MATERIALS
www.advopticalmat.de

Near-Infrared Spectrally Selective Plasmonic Electrochromic Thin Films

*Guillermo Garcia, Raffaella Buonsanti, Anna Llordes, Evan L. Runnerstrom, Amy Bergerud, and Delia J. Milliron**

The use of chromogenic materials as potential dynamic window coatings has been explored to increase building energy efficiency by optimizing solar gain.[1,2] Currently, there are four classes of responsive materials under investigation for dynamic fenestration applications: photochromic, thermochromic, gasochromic, and electrochromic.[3–6] Of these four, electrochromic materials can achieve the largest projected energy savings by providing the widest range of solar control.[5,6] Unlike traditional electrochromic materials that primarily modulate visible light, our recent results suggest that plasmonic electrochromic coatings offer a unique opportunity to selectively control the transmission of near infrared radiation (NIR) without affecting visible transparency.[7,8] Degenerately doped semiconductor nanocrystals (NCs), such as tin doped indium oxide (ITO), have well defined localized surface plasmon resonance (LSPR) in the NIR region of the solar spectrum.[9,10] When activated by an applied voltage, ITO NCs show a large spectral shift in their NIR LSPR due to electrochemical doping. Our previous work suggested that ITO NC thin films have the potential to serve as the foundation for a NIR selective plasmonic electrochromic coating.[8] In this study, we report optical switching characteristics relevant to critically examining this potential and explore aluminum doped zinc oxide (AZO) NC thin films as an alternative candidate material for this new type of coating. We compare the optical performance, switching kinetics, and cycling durability between AZO and ITO NC plasmonic electrochromic layers. Ultimately, the use of inexpensive, earth abundant materials as electrochromic coatings opens the door to low cost dynamic windows with improved energy efficiency.

To prepare these coatings, we first synthesized colloidal ITO and AZO NCs with specified size and doping level by balancing precursor reactivity and adjusting the indium/tin and aluminum/zinc content in the feedstock, respectively (**Figure 1**a,b, S1, S2, Table S1).[11,12] The resulting NCs are capped with organic ligands that facilitate dispersion in hydrophobic solvents. Transmission spectra of these dispersions reveal a well-defined LSPR peak at a position controlled by the doping level (Figure 1c). Note that the LSPR peaks for AZO NC dispersions lie in the mid-IR with an absorption tail in the NIR region.[12] The frequency of the LSPR (ω_{LSPR}) is proportional to the bulk plasmon frequency (ω_P), which varies as square root of the free carrier concentration (n),

$$\omega_{LSPR} \propto \omega_p = \sqrt{\frac{ne^2}{m\varepsilon_0}} \quad (1)$$

where n is the free electron density, e is the electron charge, m is the effective mass of the electrons, and ε_0 is the permittivity of free space.[13] Here, our synthetic variation of the elemental doping concentration manipulates n, which in turn alters ω_{LSPR}. The synthetic variation of the nanocrystal size has a smaller effect on the LSPR frequency.[13]

To evaluate electrochemical switching of NIR transmission, the NCs were processed into electrically conducting films. Deposition of uniform films by spincoating from an equal mixture of hexane/octane was facilitated by the hydrocarbon ligands capping the surface of the NCs. Within the NC film, these ligands form highly insulating barriers between adjacent NCs and thus must be removed to generate a conductive network. Thermal decomposition of the hydrocarbon ligands in air traps free carriers by inadvertent filling of oxygen vacancies, which leads to the elimination of the LSPR.[14] Thermal decomposition of the hydrocarbon ligands in an inert environment reduces visible transparency by leaving residual carbon byproducts in the NC layer, creating a dark tint across the film. Hence, two alternate and independent approaches were used to chemically remove the organic ligands from the surface. The first approach displaced the long bulky surface ligands with a smaller, volatile molecule through a mass-action exchange process that consisted of soaking the NC film in a 1M solution of formic acid (Figure S3a, S4a).[8] The second approach used a mild reactive stripping agent to remove the organic ligand from the NC surface altogether. This process was facilitated by immersing ITO and AZO NC films in a trimethyloxonium tetrafluoroborate (methyl Meerwein reagent) or triethyloxonium tetrafluoroborate (ethyl Meerwien reagent) solution for several minutes, respectively (Figure S5a, S6a).[15] For both approaches, a thermal anneal in argon was performed at 300 °C following the chemical treatment. For the formic acid exchanged films, this annealing step facilitated the desoprtion of insulating, organic material from the NC surface. The thermal treatment also led to improved NC-NC contact regardless of exchange method, leading to a conductive NC network. Both processing techniques showed no etching at the nanocrystal surface

Dr. G. Garcia, Dr. R. Buonsanti, Dr. A. Llordes, E. L. Runnerstrom, A. Bergerud, Dr. D. J. Milliron
The Molecular Foundry
Lawrence Berkeley National Laboratory
Berkeley, California, 94720, USA
E-mail: dmilliron@lbl.gov
E. L. Runnerstrom, A. Bergerud
Department of Materials Science and Engineering
University of California
Berkeley, California, 94720, USA

DOI: 10.1002/adom.201200051

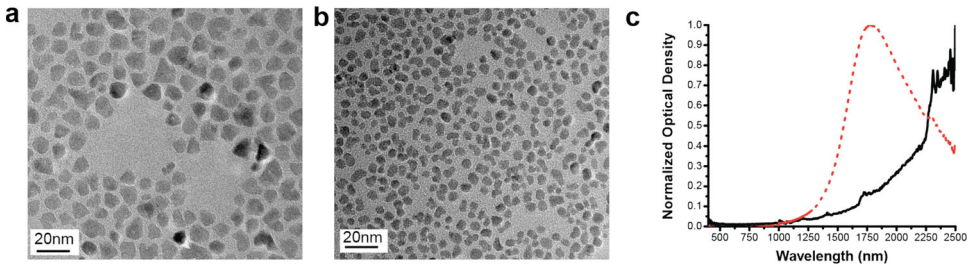

Figure 1. Transmission electron microscopy images of (a) AZO nanocrystals and (b) ITO nanocrystals with 9.0 ± 1.5 nm and 5.0 ± 1.0 nm diameter, respectively. (c) Normalized extinction spectra of the same AZO (black, solid) and ITO (red, dashed) nanocrystals with 3.7% Al and 13.1% Sn doping, respectively.

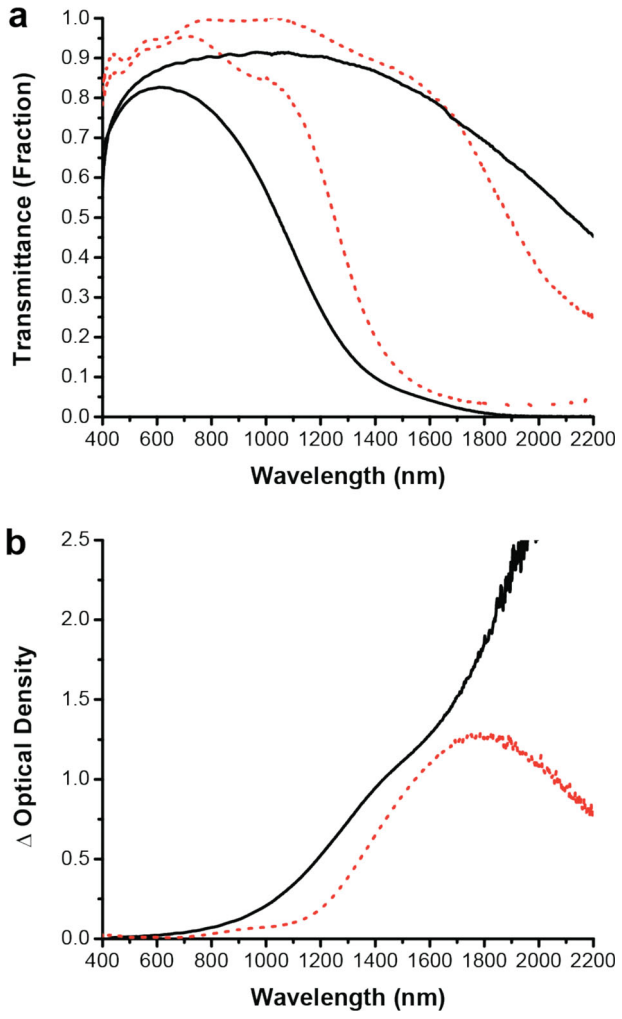

Figure 2. Optical properties of AZO (black, solid) and ITO (red, dashed) nanocrystal thin films during electrochecmical modulation. Applied voltages in the transmissive "bleached" and absorptive "colored" state are from 4 to 1.5 V and 4 to 2 V for AZO and ITO nanocrystal films, respectively. AZO and ITO thin films were composed of nanocrystals with 9.0 ± 1.5 nm and 5.0 ± 1.0 nm diameter and 3.7% Al doping and 13.1% Sn doping, respectively. (a) Transmittance in bleached and colored state for AZO and ITO nanocrystal films with 2435 ± 30 nm and 316 ± 10 nm thickness, respectively. (b) Change in optical density between the voltage extremes for AZO and ITO nanocrystal thin films. All potentials are referenced to a Li/Li^+ electrode in 0.1M $LiClO_4$ in propylene carbonate.

(Figure S3b, S4b, S5b, S6b) and generated a thin nanoporous film (Figure S5c, S6c).

To actively modulate the LSPR, formic acid treated NC films were positioned as the working electrode in an electrochemical cell and in situ transmission spectra were recorded as a function of the applied potential. Due to the onset of the strong absorption bands of the electrolyte, the in situ measurements were limited to a spectral window of 400–2200 nm. Upon applying a negative bias, the LSPR peak blue shifts reducing transmission through the NC film (**Figure 2**a). The magnitude of the LSPR shift during modulation depends on film thickness, nanocrystal size, and doping level.[8] For ITO and AZO NC thin films compared in this work, these parameters were 316 ± 10 nm, 5.0 ± 1.0 nm, 13.1% Sn-doping and 2435 ± 30 nm, 9.0 ± 1.5 nm, 3.7% Al-doping, respectively. Profilometry was used to determine film thickness, NC size was measured by collecting statistics in bright-field TEM, and doping concentration was assessed by inductively coupled plasma atomic emission spectroscopy (ICP-AES). The capability of producing ITO NCs with small diameters and high doping levels allows for large changes in NIR transmittance at sub micron film thickness. In contrast, AZO NC thin films require micron thickness to achieve large changes in NIR optical properties since synthetic limitations impose a minimum on the achievable NC size and a maximum on the electronic doping level.[12]

When driven between the extremes of applied voltage, AZO NC layers achieve larger changes in NIR transmittance than do ITO NC thin films (Figure 2b). This difference can be ascribed to two possible explanations: 1) The Al^{3+} dopant in the AZO NCs is electrochemically stable in the desired potential range, which allowed for widening of the applied voltage range to 2.5 V. By contrast, the Sn^{4+} dopant in the ITO NC thin films begins to reduce irreversibly at lower potentials in the desired potential range, limiting the total voltage window to 2 V. 2) The capability of extending the AZO NC layer thickness above the micron range without saturating the film absorbance led to a larger range of optical modulation. Conversely, the absorbance of ITO NC thin films begins to saturate above ~ 400nm thickness leading to a smaller modulation of transmittance.

The performance of these dynamic optical coatings as the basis for NIR selective plasmonic smart windows can be evaluated by convolving the transmittance spectra with the solar spectrum. **Table 1** outlines the portion of the solar spectrum transmitted when the film is in the transparent state

Adv. Optical Mater. **2013**,
DOI: 10.1002/adom.201200051

Table 1. Solar transmittance, NIR solar transmittance, and luminous solar transmittance of AZO and ITO nanocrystal thin films during electrochemical modulation shown in Figure 2. Applied voltage extremes in the transmissive "bleached" and absorptive "colored" state are 4 to 1.5 V and 4 to 2 V for AZO and ITO nanocrystal films, respectively. All potentials are referenced to a Li/Li^+ electrode in 0.1 M $LiClO_4$ in propylene carbonate.

Solar Transmittance	ITO	AZO
T_{solar} Colored	0.78	0.62
T_{solar} Bleached	0.91	0.82
$\triangle T_{solar}$	0.14	0.20
T_{solar} NIR Colored	0.56	0.38
T_{solar} NIR Bleached	0.81	0.77
$\triangle T_{solar}$ NIR	0.25	0.39
$T_{luminous}$ Colored	0.91	0.82
$T_{luminous}$ Bleached	0.93	0.85
$\triangle T_{Luminous}$	0.02	0.04

("bleached", positive bias) and blocking state ("colored", negative bias). For AZO and ITO NC electrodes, 40% and 25% solar NIR modulation is achieved between the voltage extremes with less than 4% and 2% modulation in the solar insolation visible to the human eye, respectively. Overall, a total of 20% and 14% solar modulation is achieved for AZO and ITO NC thin films, respectively. The efficiency at which electrochromic layers color (coloration efficiency, *CE*) is given by Equation (2),

$$CE = \frac{\Delta OD}{C/A} \tag{2}$$

where ΔOD is the change in optical density between the bleached and colored state, C is the amount of charge injected from the bleached to the colored state, and A is the area of coating being modulated. Typical coloration efficiencies for traditional high performance electrochromic layers, such as tungsten oxide, range from 50–80 $cm^2\ C^{-1}$ at 600 nm wavelength. The peak coloration efficiency for the present AZO and ITO NC thin films were 450 and 400 $cm^2\ C^{-1}$ at 2000 nm and 1800 nm wavelengths, respectively, which is roughly a factor of 7 higher than tungsten oxide (Figure S7). By utilizing capacitive charging, plasmonic electrochromic coatings achieve larger optical contrast with minimal charge requirements. This performance is already of interest for modulation of solar heating, with further gains potentially available by additional optimization of nanocrystal size, chemical doping level, and film thickness.

Switching kinetics during electrochemical modulation provide insight into the physical processes accompanying switching and are of practical importance in smart window applications as they determine the speed at which coatings can adjust to environmental changes. We hypothesized that larger concentrations of smaller ions in the electrolyte would provide the best conditions for fast switching kinetics. To investigate this hypothesis we used potential step experiments to determine the switching speed of plasmonic electrochromic color change for a variety of electrolyte conditions (Figures S8 and S9). **Table 2** outlines half-life switching times between the voltage extremes of Meerwein treated NC thin films in 0.1 M and 1 M concentrations of $LiClO_4$ or tetrabutylammonium perchlorate (TBAP) in propylene carbonate (PC). For both AZO and ITO NC thin films, larger concentrations of electrolyte led to faster switching times, regardless of the electrolyte composition. This is consistent with faster double layer reorganization at elevated ion concentrations, which is caused by shorter Debye screening lengths at higher electrolyte concentrations.[16] NC thin films had slower kinetics in $LiClO_4$ electrolytes when compared to TBAP for both AZO and ITO coatings. This result is initially counter-intuitive. However, it can be rationalized by understanding how PC solvates the electrolyte cations. In the Li^+ case, it is well understood that PC coordinates strongly, which expands the effective size of the ion during electrochemical modulation.[17–19] This increase in ion diameter affects the switching kinetics by reducing the mobility of ion within the film. Conversely, PC does not coordinate TBA^+ strongly, which allows the ion to insert into the film without its primary solvation ring. At lower concentrations of Li^+ electrolytes (0.1 M), bleaching times were longer than coloring for both AZO and ITO NC thin films. When applying a negative bias across the film, Li^+ ions enter the film pores from the bulk liquid electrolyte. The speed at which the ions fill the pores is facilitated by the mobility in the bulk electrolyte. On the other hand, when a positive bias is applied, the speed of switching is limited by the ion mobility within the pore, which is lowered by an increase of ion-ion collisions.[20] Increasing the concentration to 1 M, the reduced mobility in the pore is overcome by the smaller Debye screening length, leading to coloring and bleaching times that are approximately equal.[21] The larger pore size of AZO NC thin films, a consequence of larger diameter NCs, led to faster half life switching times than ITO NC thin films (Figure S5c and S6c). This improvement in speed is caused by an enhancement in ion chemical diffusion, which reduces the charge compensation time.[21] Overall, the half life switching time for AZO and ITO NC thin films in all electrolyte cases occurs in a matter of seconds or less. Although ion transport appears to limit switching speed for low electrolyte concentrations, at higher concentrations the resistance associated with electron hoping across the NC-NC interfaces throughout the film may limit the overall switching kinetics.[22–24] Note that when deposited on glass, both AZO and ITO NC thin films showed very high sheet resistance (Table S2). Reducing the resistance at the NC-NC interface would improve the achievable switching speed.

Table 2. Half-life switching times of ITO and AZO nanocrystal thin films during electrochemical modulation. The applied voltage extremes between the colored and bleached state are –0.8 to 1.2 V and –1.3 to 1.2 V for the ITO and AZO nanocrystal thin films, respectively. The half-life switching times are reported for two electrolyte concentrations (0.1 M and 1 M) of $LiClO_4$ and tetrabutylammonium perchlorate (TBAP) in propylene carbonate. All potentials are referenced to the normal hydrogen electrode (NHE) and all samples are deposited on ITO glass substrates with 20 ± 5 Ω sheet resistance. AZO and ITO thin films were composed of nanocrystals with 12.9 ± 2.0 nm and 5.0 ± 1.0 nm diameter and 3.8% Al doping and 13.1% Sn doping, respectively.

Electrolyte	AZO Coloration [s]	AZO Bleaching [s]	ITO Coloration [s]	ITO Bleaching [s]
0.1M $LiClO_4$	0.50	0.90	1.53	3.40
1M $LiClO_4$	0.19	0.16	0.28	0.30
0.1M TBAP	0.10	0.11	0.24	0.23
1M TBAP	0.07	0.06	0.05	0.06

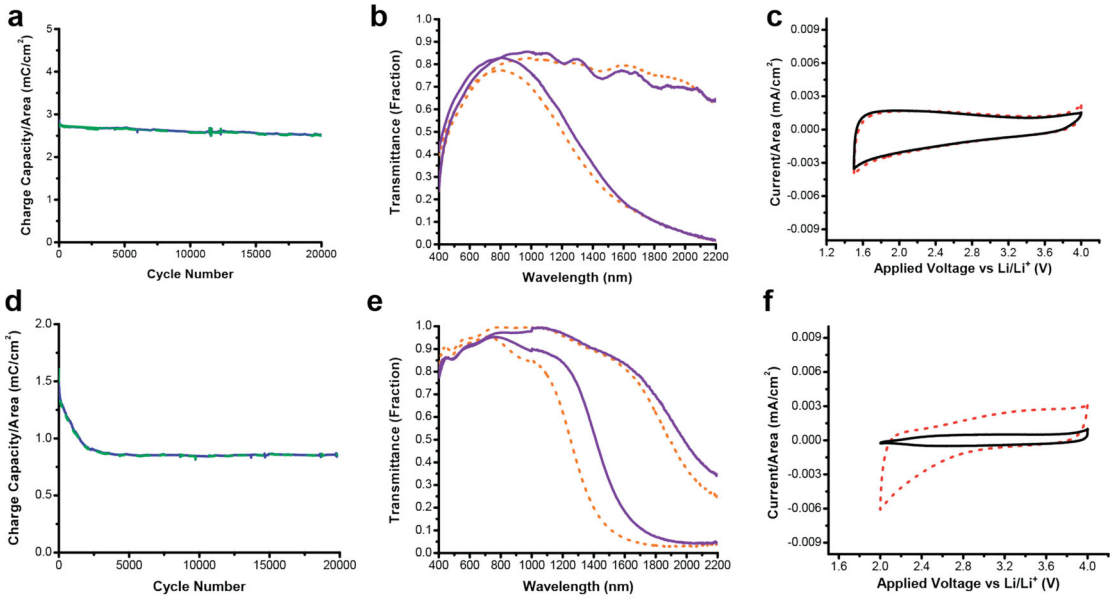

Figure 3. Lifetime durability testing of AZO and ITO nanocrystal thin films. Charge capacity showed little variation between charging (blue, solid) and discharging (green, dashed) but was reduced by 11% and 45% for AZO (a) and ITO (d) coatings, respectively, after 20 000 cycles between the applied voltage extremes. Optical properties and cyclic voltammograms for AZO (b,c) and ITO (e,f) coatings before (orange, red, dashed) and after 20 000 cycles (purple, black, solid) show no significant effect in optical/charge capacity performance for AZO layers but reduced the optical modulation/charge capacity of ITO coatings, respectively. AZO and ITO coatings were composed of nanocrystals with 12.9 ± 2.0 nm and 5.0 ± 1.0 nm diameter and 3.8% Al doping and 13.1% Sn doping, respectively. Applied voltage in the bleached and colored state are 4 V to 1.5 V and 4 V to 2 V for AZO and ITO nanocrystal films, respectively. All potentials are referenced to a Li/Li^+ electrode in 0.1 M $LiClO_4$ in propylene carbonate. Cyclic voltammograms scan rates are 10 mV/s and 1 mV/s for AZO and ITO nanocrystal thin films, respectively. Charge capacity scan rates used for durability testing are 60mV/s for both AZO and ITO.

Stability under repeated cycling is an important requirement for electrochromic switching as it determines the maximum lifetime of the contemplated device. Durability tests performed on Meerwein treated AZO and ITO NC thin films showed an 11% and 45% reduction in charge capacity after cycling 20,000 times between the applied voltage extremes in a $LiClO_4$ in PC electrolyte (**Figure 3**a,3d). This loss in charge compensation did not significantly affect the optical performance of AZO NC thin films but reduced the optical modulation range of ITO NC coatings (Figure 3b,3e). Cyclic voltammograms of NC thin films before and after cycling 20,000 times showed only a slight change in charge injection for AZO coatings but did show a substantial loss in charge injection for ITO thin films during modulation (Figure 3c,3f). To investigate the origin of these differences in cycling performance, XPS of ITO NC thin films before and after 20,000 cycles was performed. It was determined that partial reduction of the Sn^{4+} to Sn^{2+} occurred during cycling (Figure S10). It was further seen that ITO NC coatings have a lower charge capacity when switched in the TBAP electrolyte (Figure S11c).[25,26] TBA^+ is physically too large to insert into the crystalline lattice, leaving only capacitive contributions, while the additional charge when cycling in $LiClO_4$ can be ascribed to Li^+ insertion reactions. We suggest that Li^+ insertion facilitates the partial irreversible reduction of Sn^{4+} over many cycles.[27] This leads to an overall decline in optical performance both in the visible and NIR as cycling proceeds (Figure S11d). On the other hand, cyclic voltammograms of AZO NC thin films in TBAP and $LiClO_4$ electrolytes showed no difference in charge capacity and optical performance during modulation, consistent with capacitive charging of AZO and the electrochemical stability of Al^{3+} (Figure S11a, S11b).

This study demonstrates the potential of using Al-doped ZnO, an earth abundant, inexpensive material, for near-infrared selective plasmonic electrochromic windows. Here, we showed enhanced NIR optical contrast, switching kinetics, and cycling durability for AZO NC thin films compared to ITO NC layers. Slight reduction of Sn in ITO NC thin films during cycling limited the optical performance and the lifetime of the device. Switching times between applied voltage extremes are roughly one hundred milliseconds even with the high electronic resistance in the NC networks. Overall, the use of degenerately doped semiconductor nanocrystals for near infrared plasmonic electrochromic coatings will open the door for enhanced energy performance in low cost smart window applications.

Experimental Section

Materials –ITO: Indium acetylacetonate ($In(acac)_3$, 99.99%), tin acetate ($Sn(Ac)_4$ 99.99%), myristic acid (MA, ≥ 98%), 1-octadecene (ODE, 90%), and oleic acid (OLAC, 90%) were purchased from Aldrich and used without further purification. Oleylamine (OLAM, 90%) was obtained from Acros.

Materials – AZO: Zinc Stearate ($ZnSt_2$, technical grade), aluminum acetylacetonate (Al(acac)3, 99%), oleic acid (OLAC, 90%), 1-octadecene (ODE 90%), 1,2-hexadecanediol (1,2HDDIOL 90%) were purchased from Aldrich and used without further purification.

Adv. Optical Mater. **2013**,
DOI: 10.1002/adom.201200051

Synthetic Methods –ITO: ITO NCs doped with 13.1% of Sn (Figure 1b in the manuscript): $In(acac)_3$ (1 mmol), $Sn(acac)_4$ (0.2 mmol), and MA (3 mmol) were mixed with 20 mL of ODE in a three-neck flask and degassed under vacuum at 110 °C for 2 h. Afterwards, the temperature was increased to 295 °C and 1 mL of a previously degassed 3M solution of OLAM in ODE was rapidly injected. The solution temperature dropped to 280 °C and was maintained for 1h. The solution became yellow in color almost instantaneously, later turning to orange and finally dark green within 10 minutes of the injection. The temperature was then further reduced to 240 °C for an additional 1 h. The NCs were collected by adding 10 mL of chloroform to the final reaction mixture and precipitating with ethanol. Further precipitation and washing were performed with hexane/ethanol. Finally, the NCs were dispersed in a 1:1 mixture of octane:hexane.

Synthetic Methods – AZO: A solution (A) containing $ZnSt_2$ (1 mmol), $Al(acac)_3$ (0.25 mmol), OLAC (3 mmol) in 4 mL of ODE and a mixture (B) of 1,2-HDDIOL (10 mmol) in 11 mL ODE were loaded in three-neck flasks and magnetically stirred at 140 °C under argon for 1 h. Afterward, the temperature in B was increased to an injection temperature *Tinj* (*Tinj* = 260 °C and 245 °C for the 13 nm and 9 nm AZO NCs, respectively) and solution A was rapidly injected into B, which was accompanied by a temperature drop $\Delta T \approx 20$ °C (*Tgrowth* = *Tinj* – ΔT). After 5 hours at *Tgrowth*, the reaction mixture was allowed to cool. Ethanol was added (a white flocculate from the clear yellow-orange solution was generally only observed for the largest NCs) and the NCs were separated from the reaction mixture by centrifugation (9000 rpm for 20 min). After two cycles of redispersion in hexane (1 mL) and reprecipitation by ethanol, 20–30 mg of precipitate was eventually collected and dispersed in 800 µL of a 1:1 hexane:octane mixture.

Elemental Analysis: Elemental analysis was performed by induced coupled plasma atomic emission spectroscopy (ICP-AES) with a Varian 720/730 Series spectrometer. The AZO and ITO samples were digested in concentrated HCl. The relative error on the extracted Sn and Al content was within 3% of the reported percentage, as evaluated on the basis of 9 replicates per each measurement.

Morphological Analysis: Low- and high-resolution TEM were carried out on a JEOL 2100 microscope, at an accelerating voltage of 200 kV. Samples for TEM analysis were prepared by drying a drop of hexane solution containing the NCs on the surface of an ultra-thin carbon-coated copper grid.

Film Preparation: A spin-casting technique was used to generate thin films of ITO and AZO nanocrystals. Transparent conducting oxide (TCO) substrates were cleaned via sonication in a three step process: 15 min de-ionized water with 2% Hellmanex solution, 15 min acetone, 15 min isopropanol. Three rinses were performed between each sonication step. Using a one to one octane/hexane solution of ITO and AZO NCs (~60–70 mg/mL), 30 µL were dispensed on a 2 cm × 2 cm TCO substrate. The spinning recipe consisted of an initial 1000 RPM spin for 30 seconds followed by a 4000RPM spin for 20 seconds. In situ ligand exchange was performed on the nanocrystal films by immersing them in a 1 M formic acid/acetonitrile solution or 20 mM Meerwein/acetonitrile for 45 min. Meerwein exchanges were carried out in anhydrous solvent within a nitrogen glove box. The methyl based Meerwein salt (Me_3OBF_4) was used for ITO samples and the ethyl based Meerwien salt ($(CH_3CH_2)_3OBF_4$) was used for AZO samples. Samples were rinsed with acetonitrile and dried with a nitrogen gun prior to thermal treatment. All samples were heated in an argon environment at 300 °C for 30 min. The entire process was repeated for additional layers to increase film thickness. Film edges were cut off from samples using a diamond tip scribe to eliminate regions of poor uniformity created from spincoating.

Film Characterization: Film thickness was measured between each post processing step using a Veeco Dektak 150+ Profiler and confirmed with 90 degree cross section images using a Zeiss Gemini Ultra-55 Analytical Scanning Electron Microscope. Material characteristics were checked between post processing steps using a Bruker D8-Discover X-ray diffractometer equipped with a GADDS area detector and operated at 40 kV and 20 mA at the wavelength of Cu Kα, 1.54 Å.

Electrochemical Measurements: Prepared films were immersed in an anhydrous 0.1 M or 1 M lithium perchlorate/propylene carbonate electrolyte solution for electrochemical measurements. Separate lithium foils were used for counter and reference electrode. The films were driven at a potential range of 1.5 to 4V and 2 to 4 V versus the Li reference electrode for AZO and ITO NC thin films, respectively. In situ optical spectra were taken of the films at potential extremes. These were collected after allowing for stabilization of the optical response. The optical pathlength through the electrolyte was ~2 mm during measurements. Charge and transport measurements between the potential limits were performed using a chronopotentiometry technique with a 10 µA sourced current. Five cycles were performed in each measurement and a final value was averaged out from the set. Film cycling was performed using a cyclic voltammetry technique. Films were cycled between the potential limits at 60 mV/s for durability test and at 1 and 10 mV/s scan rates for charge measurements. Electrochemical measurements were repeated with an anhydrous 0.1M and 1M tetrabutylammonium perchlorate (TBAP)/acetonitrile electrolyte. In this set up, a platinum wire was used as a counter electrode. A Ag/Ag^+ reference electrode consisting of a silver wire immersed in a 0.01M $AgNO_3$/0.1M TBAP/acetonitrile solution was used as a reference electrode. The films were driven between a potential range of –1.55 and 0.95 V and –1.05 to 0.95 V versus the reference electrode for AZO and ITO NC thin films, respectively, in order to match the conditions set by the lithium based electrolyte. Coloration efficiency was calculated by taking the ratio of the change in optical density between the positive and negative bias with its associated charge per unit area. All electrochemical measurements were performed in an argon glove box with a Bio-logic VSP potentiostat and a ASD Quality Spec Pro VIS/NIR spectrometer.

Supporting Information

Supporting Information is available from the Wiley Online Library or from the author.

Acknowledgements

Research was supported by the U.S. Department of Energy (DOE) under Contract No. DE-AC02–05CH11231, including work performed at the Molecular Foundry as a user project and a DOE Early Career Research Program grant (Dr. Garcia and Dr. Milliron). Mr. Runnerstrom and Ms. Bergerud were supported by a Chancellor's Fellowship for Graduate Study. Ms. Bergerud is also supported by a National Science Foundation Graduate Student Research Fellowship under Grant No. DGE 1106400.

Author Contributions

G.G., R.B, E.L.R., and A.L. prepared and characterized NC materials and films; G.G. performed electrochemical characterization; A.B. performed XPS measurements and analysis; D.J.M. provided guidance on experimental design and interpretation; D.J.M. designed and oversaw all aspects of the project. All authors contributed to the manuscript preparation.

Received: November 30, 2012
Revised: January 19, 2012
Published online:

[1] United Nations Environmental Programme (UNEP), *Buildings and Climate Change: Status, Challenges and Opportunities*, Paris, France **2007**.
[2] B. P. Jelle, A. Hynd, A. Gustavsen, D. Arasteh, H. Goudey, R. Hart, *Sol. Energy Mater. Sol. Cells* **2012**, *96*, 1–28.

[3] R. Baetens, B. P. Jelle, A. Gustavsen, *Sol. Energy Mater. Sol. Cells* **2010**, *94*, 87–105.
[4] P. Bamfield, M. G. Hutchings, *Chromic Phenomena: Technical Applications of Colour Chemistry*. RCS Publishing, Cambridge, UK **2010**.
[5] S. Y. Li, G. A. Niklasson, C. G. Granqvist, *Thin Solid Films* **2012**, *520*, 3823–3828.
[6] C. G. Granqvist, S. Green, G. A. Niklasson, N. R. Mlyuka, S. Von Kraemer, P. Georen, *Thin Solid Films* **2010**, *518*, 3046–3053.
[7] E. S. Lee, S. E. Selkowitz, R. D. Clear, D. L. DiBartolomeo, J. H. Klens, L. L. Fernandez, G. J. Ward, V. Inkarojrit, M. Yazdanian, *Advancement in Electrochromic Windows CEC-500–2006–052*, California Energy Commission, PIER, Lawrence Berkeley National Laboratory, Berkeley, CA **2006**.
[8] G. Garcia, R. Buonsanti, E. L. Runnerstrom, R. J. Mendelsberg, A. Llordes, A. Anders, T. J. Richardson, D. J. Milliron, *Nano Letters* **2011**, *11*, 4415–4420
[9] M. Kanehara, H. Koike, T. Yoshinaga, T. Teranishi, *J. Am. Chem. Soc.* **2009**, *131*, 17736–17737.
[10] S. C. Warren, D. A. Walker, B. A. Grzybowski, *Langmuir* **2012**, *28*, 9093–9102.
[11] R. A. Giltsrap, C. J. Capozzi, C. G. Carson, R. A. Gerhardt, C. J. Summers, *Adv. Mater.* **2008**, *20*, 4163–4166.
[12] R. Buonsanti, A. Llordes, S. Aloni, B. A. Helms, D. J. Milliron, *Nano Lett.* **2011**, *11*, 4706–4710.
[13] S. Link, M. A. El-Sayed, *J. Phys. Chem. B.* **1999**, *103*, 8410–8426.
[14] N. Yamada, I. Yasui, Y. Shigesato, H. Li, Y. Ujihira, K. Nomura, *Jpn. J. Appl. Phys.* **2000**, *39*, 4158–4163.
[15] E. L. Rosen, R. Buonsanti, A. Llordes, A. M. Sawvel, D. J. Milliron, B. A. Helms, *Angew. Chem. Int. Ed.* **2012**, *51*, 684–689.
[16] A. J. Bard, L. R. Faulkner, *Electrochemical Methods: Fundamentals and Applications* Wiley, Hoboken, NJ **2000**.
[17] D. Aurbach, M. D. Levi, E. Levi, A. Schechter, *J. Phys. Chem. B.* **1997**, *101*, 2195–2206.
[18] Y. Kameda, Y. Umebayashi, M. Takeuchi, M. A. Wahab, S. Fukuda, S. Ishiguro, M. Sasaki, Y. Amo, T. Usuki, *J. Phys. Chem. B.* **2007**, *111*, 6104–6109.
[19] H. Zhang, C. Sun, F. Li, C. Liu, J. Tan, H. Cheng, *J. Phys. Chem. C.* **2007**, *111*, 4740–4748.
[20] C. Masarapu, L. Wang, X. Li, B. Wei, *Adv. Energy Mater.* **2012**, *2*, 546–552.
[21] J. Bisquert, *Phys. Chem. Chem. Phys.* **2008**, *10*, 49–72.
[22] D. Vanmaekelbergh, P. Liljeroth, *Chem. Soc. Rev.* **2005**, *34*, 299–312.
[23] P. Guyot-Sionnest, *J. Phys. Chem. Lett.* **2012**, *3*, 1169–1175.
[24] A. Zabet-Khosousi, A. Dhirani, *Chem. Rev.* **2008**, *108*, 4072–4124.
[25] U. Zum Felde, M. Haase, H. Weller, *J. Phys. Chem. B* **2000**, *104*, 9388–9395.
[26] M. Pflughoefft, H. Weller, *J. Phys. Chem. B* **2002**, *106*, 10530–10534.
[27] C. A. Huang, K. C. Li, G. C. Tu, W. S. Wang, *Electrochim. Acta* **2003**, *48*, 3599–3605.

Adv. Optical Mater. **2013**,
DOI: 10.1002/adom.201200051